Clay Minerals (2024), **59**, 39–49
doi:10.1180/clm.2024.5

CAMBRIDGE UNIVERSITY PRESS

Article

Natural and pretreated Gördes clinoptilolites for ammonia removal: effect of exchangeable cations (Na^+, K^+, Ca^{2+} and Mg^{2+})

Burcu Erdoğan and Orkun Ergürhan
Department of Physics, Faculty of Science, Eskisehir Technical University, Eskisehir, Türkiye

Abstract

In this study, the effects of two different ammonium-exchange methods to improve the ammonia (NH_3) gas adsorption of raw clinoptilolite (CLN) from Gördes (Türkiye) was investigated. The first method involved direct modification of CLN by 0.5 or 1.0 M NH_4NO_3 solutions at 80°C for 4 and 8 h followed by calcination. In the second method, CLN was converted to the Na^+ form prior to modification with ammonium nitrate and calcination under the same conditions. Both methods yielded H^+ forms of CLN through the removal of exchangeable cations without damaging the crystal structure. Ammonia adsorption isotherms were determined at 298 K for a total of eight different H^+ forms synthetized using both methods. The Na-1.0-8h CLN sample with the highest NH_3 adsorption capacity obtained using the second method was selected as the parent CLN. In addition, to determine the effects of doping different cations into the structure on the NH_3 adsorption properties of the selected parent CLN sample, cation-exchange processes were carried out using 0.5 and 1.0 M $NaNO_3$, KNO_3, $Ca(NO_3)_2$ and $Mg(NO_3)_2$ solutions at 80°C for 4 h. The raw and modified CLNs were characterized using X-ray diffraction, X-ray fluorescence, scanning electron microscopy and N_2 adsorption analyses. Cation-exchanged samples with a wide range of NH_3 adsorption capacities (3.61–4.93 mmol g^{-1}) were compared with other zeolites from the literature.

Keywords: Adsorption; ammonia; BET; clinoptilolite; XRD; XRF

(Received 4 November 2023; revised 13 February 2024; accepted 13 February 2024; Accepted Manuscript online: 26 February 2024; Editor: George E. Christidis)

The quality and chemistry of the Earth's atmosphere are critical to the future of human and mammalian life. Since the beginning of humankind's industrial activity, the chemical composition of the atmosphere has changed due to the release of volatile pollutants and greenhouse gases (Fowler, 2020). Ammonia (NH_3), an irritating, malodorous and colourless gas, is one of these pollutants. Ammonia is used as an ingredient in many commercial cleaning and pharmaceutical products, as a hydrogen carrier and as a fertilizer (Kobayashi, 2019; Sun *et al.*, 2021) and for selective catalytic reduction of NO_x (Li *et al.*, 2011; Wang *et al.*, 2017). Large amounts of ammonia are released into the atmosphere from livestock farming and agricultural activities (Ciahotný, 2002). This ammonia release can be taken up by atmospheric moisture and surface water and also accumulate in plants and soil (Renard, 2004). Changes in atmospheric ammonia concentrations are known to have adverse effects on the environment (Amon, 1997). In addition, exposure to certain levels of ammonia can be extremely harmful to human health. Inhaled ammonia is mainly absorbed by water in human tissues, denaturing proteins and eventually destroying cell membranes (Sun *et al.*, 2021). This can cause nausea, coughing, dizziness, pulmonary oedema and weakening of the immune system (Lindgren, 2010; Sun *et al.*, 2021). Therefore, indoor ammonia concentrations can also pose a threat to the health of workers. For example, workers who work in an environment with high levels of ammonia are at risk of developing chronic respiratory diseases such as bronchial asthma (Ballal, 1998). Ammonia can also affect the reproductive functioning of female workers (Sun *et al.*, 2021). Animals in livestock buildings are also affected by the presence of ammonia in the environment. Hence, inflammatory responses are observed in the respiratory system of pigs exposed to ammonia concentrations of 100 and 150 ppm (Drummond, 1980). It is therefore clear that indoor ammonia levels also need to be controlled.

Many porous adsorbents such as metal–organic frameworks, covalent organic frameworks, hydrogen-bonded organic frameworks, porous organic polymers and their composite materials have been studied for their ability to remove ammonia (Won Kang *et al.*, 2020). One such adsorbent is zeolite, an Al-silicate mineral found in nature or synthesized in the laboratory. The framework of the zeolites is formed by the combination of tetrahedral silicate $[SiO_4]^{4-}$ units. Combinations of these units form channels or networks. During the formation of zeolites, the isomorphic substitution of a trivalent cation, namely Al^{3+} or Ga^{3+} for Si^{4+}, creates a negative charge that is balanced by the presence of exchangeable cations such as Na^+, Mg^{2+} and Ca^{2+}, amongst others (Gottardi & Galli, 1985). Clinoptilolite (CLN), a natural zeolite, is a member of the heulandite (HEU) group. The general formula of CLN is $(Na,K)_6(Al_6Si_{30}O_{72})\cdot 20H_2O$. Its framework structure of monoclinic C_2/m symmetry with the unit cell parameters $a = 17.62$ Å, $b = 17.91$ Å, $c = 7.39$ Å and $\beta = 116°16'$ is almost identical to that of HEU. However, CLN has a higher Si/Al ratio (≥4) and is more thermally stable than HEU (Mumpton, 1960; Ward & McKague, 1994). CLN has a two-

Corresponding author: Burcu Erdoğan; Email: burcuerdogan@eskisehir.edu.tr
Cite this article: Erdoğan B, Ergürhan O (2024). Natural and pretreated Gördes clinoptilolites for ammonia removal: effect of exchangeable cations (Na^+, K^+, Ca^{2+} and Mg^{2+}). *Clay Minerals* **59**, 39–49. https://doi.org/10.1180/clm.2024.5

dimensional channel network (10-membered A and 8-membered B channels run along the *a*-axis whilst 8-membered C channels intersect them along the *c*-axis; Ambrozova, 2017). In addition to its catalytic (Dziedzicka *et al.*, 2016) and medical (Mastinu *et al.*, 2019) applications, CLN is used for the removal of heavy metal ions (Zendelska *et al.*, 2018; Elboughdiri, 2020; El-Arish *et al.*, 2022), of environmental pollutants from wastewater (Shamshiri *et al.*, 2022) and of toxic gases from air (Macala *et al.*, 2009; Karousos *et al.*, 2016; Ghahri *et al.*, 2017; Senila, 2022).

It is common to apply chemical processes such as treatment with acid (H_2SO_4, H_3PO_4 and HNO_3) and salt (KNO_3, $NaNO_3$ and $Mg(NO_3)_2$) solutions to improve the physicochemical and gas adsorption properties of natural zeolites (Christidis *et al.*, 2003; Ciahotný *et al.*, 2006; Erdoğan Alver & Sakızcı 2019). However, even at low molarities, dealumination during hydrochloric acid treatment causes the crystal structure to collapse rapidly (Christidis *et al.*, 2003; Garcia-Basabe *et al.*, 2010). An alternative method to modify the structure of CLN is calcination after ammonium (NH_4^+) exchange. In this process, raw CLN is treated with ammonium salt solution, and the obtained product (or sample) is calcined at temperatures of 400–600°C for 2–8 h. In this way, ammonium ions adsorbed from the salt solution decompose into ammonia and hydrogen ions. As a result, H^+-CLN with a higher surface area than the raw material can be obtained without disrupting the structure (Rožić *et al.*, 2005; Allen *et al.*, 2009). In the literature, there are many studies in which H^+ forms of CLN were obtained using different calcination temperatures and various molarities of ammonium salt solutions (Kurama *et al.*, 2002; Elysabeth *et al.*, 2019; Liao *et al.*, 2019; Hieu *et al.*, 2022). However, it remains to be investigated how the ammonia adsorption properties of CLN in the H^+ form obtained after calcination change after modification with different cations. Therefore, the main objective of this study is to determine the ammonia adsorption capacity of H^+-CLN synthesized by calcination after direct and indirect ammonium nitrate exchange and to select the most suitable parent sample in terms of ammonia retention. As a second objective of this study, the effect of doping the selected parent sample with K^+, Na^+, Mg^{2+} and Ca^{2+} cations on the ammonia adsorption efficiency was investigated.

Experimental

Materials and methods

Gördes CLN (Esenli & Sirkecioğlu, 2005; Esenli *et al.*, 2023) was sieved with a sieving machine (Retsch, Germany) to obtain <125 μm fraction and split to 5.0 g aliquots. To remove soluble impurities, each zeolite aliquot was kept in 100 mL deionized water at 80°C for 4 h. All samples were then separated and washed several times with hot distilled water. Two different methods were used to synthesize the H^+-zeolites (Fig. 1). In Method 1, by which H^+ forms were obtained directly, the samples were modified with 100 mL of 0.5 and 1.0 M NH_4NO_3 solutions at 80°C for 4 and 8 h, respectively. The H^+ forms obtained by calcining these samples at 400°C for 6 h were labelled as 0.5-4h-CLN, 0.5-8h-CLN, 1.0-4h-CLN and 1.0-8h-CLN (Fig. 1).

In Method 2, by which H^+ forms were obtained indirectly, CLN samples were first modified with 100 mL of 1.0 M $NaNO_3$ solution at 80°C for 4 h. All samples were then filtered, washed several times with hot distilled water and dried at room temperature. These samples were then modified with 100 mL of 0.5 and 1.0 M NH_4NO_3 solutions for 4 and 8 h and calcined at 400°C for 6 h to indirectly obtain the H^+-zeolites. These samples were labelled as Na-0.5-4h-CLN, Na-0.5-8h-CLN, Na-1.0-4h-CLN, and Na-1.0-8h-CLN (Fig. 1). For all cation-exchange procedures, 5.0 g of the CLN sample was used per 100 mL of solution. Ammonia adsorption measurements of these different H^+-CLN samples obtained using both methods were carried out at 298 K. The Na-1.0-8h-CLN sample with the highest ammonia adsorption capacity among the H-forms (prepared using Method 2) was selected as the main CLN for further experiments. In the second step after the selection of the parent sample, 5.0 g of each parent CLN sample was exchanged with 0.5 and 1.0 M $NaNO_3$, KNO_3, $Ca(NO_3)_2$ and $Mg(NO_3)_2$ solutions at 80°C for 4 h to investigate the effect of doping the structure of this sample with different cations on the ammonia adsorption capacity. The cation-exchanged samples of the parent sample were then separated and washed several times with deionized water at boiling point, and the dried samples were kept in an oven at 100°C for 12 h and stored in a desiccator. Finally, the cation-exchanged samples of the parent sample were labelled as 0.5-Na-CLN, 0.5-K-CLN, 0.5-Ca-CLN, 0.5-Mg-CLN, 1.0-Na-CLN, 1.0-K-CLN, 1.0-Ca-CLN or 1.0 Mg-CLN depending on the salt solution used in the cation-exchange process.

Instrumentation

The original and cation-exchanged CLN samples were characterized by X-ray fluorescence (XRF), X-ray diffraction (XRD), scanning electron microscopy (SEM) and N_2 adsorption techniques. Elemental analyses of the samples were performed using a Rigaku ZSX Primus instrument. Loss on ignition (LOI) was determined by mass measurement after heating at 1000°C at a heating rate of 10°C min^{-1}, before being allowed to stand for 1 h and then cooled to room temperature at the same rate. Powder XRD traces were obtained on a Bruker D8 Advance instrument using Cu-*K*α ($\lambda = 1.54$ Å) radiation at 40 kV and 40 mA in the range 5–40°2θ, with a scanning step of 0.02°2θ. SEM images were recorded with a Zeiss Ultra Plus field emission scanning electron microscope (FE-SEM) at a 5 kV acceleration voltage. All samples were gold coated prior to analysis. Specific surface areas and micropore data were obtained from the N_2 adsorption isotherms. Ammonia adsorption isotherms were measured at 298 K to 100 kPa for all samples. The N_2 and NH_3 adsorption analyses of the CLNs were performed using a 3Flex volumetric apparatus (Micromeritics) after degassing at 300°C for 8 h.

Results and discussion

Elemental analysis

The results of the XRF analysis of the raw CLN, parent CLN and the cation-exchanged forms (0.5-Na-CLN, 0.5-K-CLN, 0.5-Ca-CLN, 0.5-Mg-CLN, 1.0-Na-CLN, 1.0-K-CLN, 1.0-Ca-CLN and 1.0-Mg-CLN) are listed in Table 1. Raw CLN is rich in potassium and calcium and has a SiO_2/Al_2O_3 ratio of 5.7. Compared to the raw material, the parent sample prepared using Method 2 showed significant changes in its chemical composition and significant removal of exchangeable cations from the structure without damaging the crystal structure, as was confirmed by the XRD data. Prior to calcination, the cation exchange of extra-framework cations (Na^+, K^+, Ca^{2+} and Mg^{2+}) with NH_4^+ resulted in significant reductions in the CaO and K_2O components.

The cation-exchanged forms of the parent CLN had higher contents of those oxides according to the salt solutions and the

https://doi.org/10.1180/clm.2024.5 Published online by Cambridge University Press

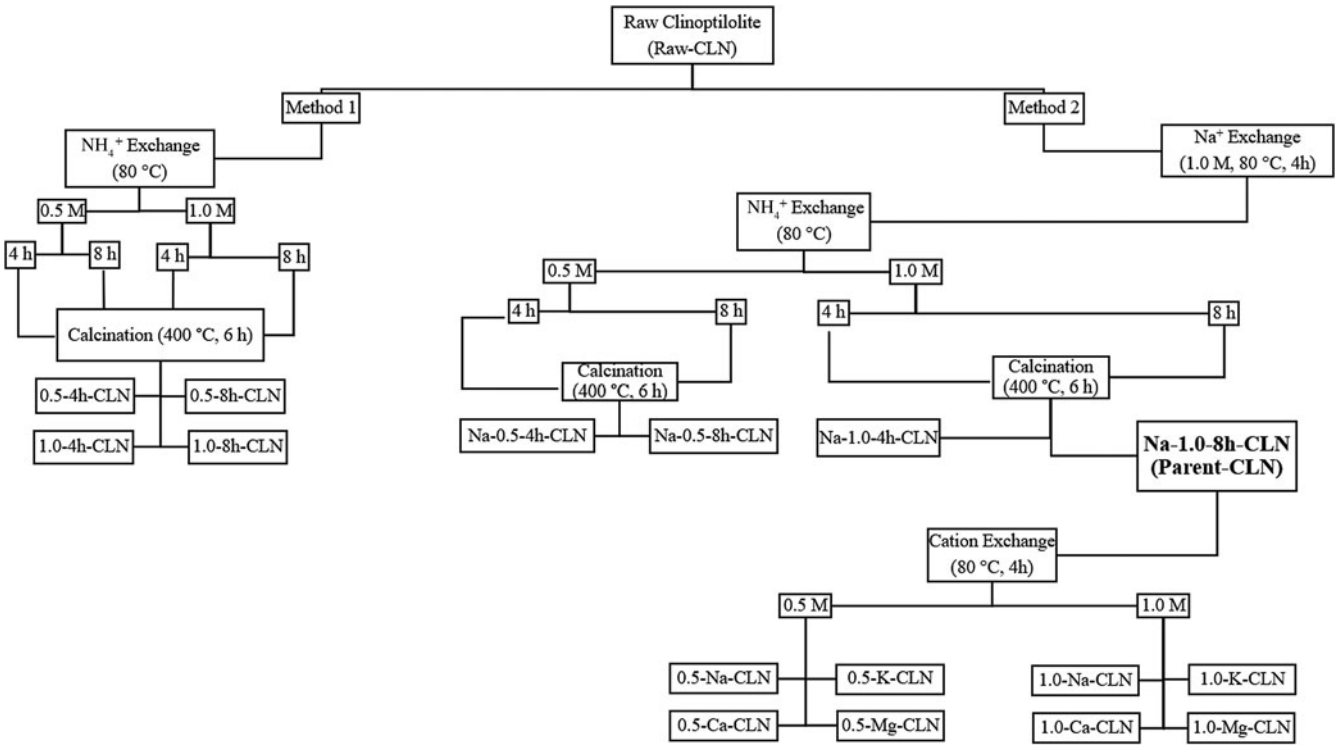

Figure 1. Schematic diagram of the sample preparation procedure.

increasing molarity of this solution (Table 1). As Method 2, which was used to obtain the parent sample, did not damage the crystal structure and did not cause dealumination, there were no significant changes in the SiO_2/Al_2O_3 ratios of the parent sample and those of cation-exchanged forms compared to the raw CLN.

XRD analysis

The powder XRD traces of the raw CLN, parent CLN, 0.5-Na-CLN, 0.5-K-CLN, 0.5-Ca-CLN, 0.5-Mg Na-CLN, 1.0-CLN, 1.0-K-CLN, 1.0-Ca-CLN and 1.0-Mg-CLN samples are shown in Fig. 2. The characteristic peaks of CLN for the raw CLN sample were observed at 9.88°, 11.17°, 22.50° and 32.01°2θ, corresponding to $d = 8.95$, 7.91, 3.96 and 2.79 Å, with *hkl* indices of (020), (200), (131) and (530), respectively (Moore & Reynolds Jr, 1997). In addition to CLN (80–85%), small amounts of feldspar (3%), opal-A (5–10%) and illite (2%) are also present in the raw CLN sample (quantitative analysis according to Esenli & Sirkecioğlu, 2005). The positions of the main CLN peaks did not changed significantly after cation exchange (Fig. 2).

Table 1. Chemical composition (wt.%) for raw CLN and parent CLN and its cation-exchanged forms.

Sample	SiO_2	Al_2O_3	Fe_2O_3	MgO	CaO	Na_2O	K_2O	LOI	SiO_2/Al_2O_3
Raw CLN	71.85	12.56	0.82	0.50	1.91	1.04	4.86	6.42	5.7
Parent-CLN	74.68	13.15	0.85	0.22	0.20	0.62	1.83	8.44	5.7
0.5-Na-CLN	74.53	12.91	0.75	0.20	0.22	2.71	1.57	7.07	5.8
1.0-Na CLN	73.96	12.74	0.78	0.24	0.23	3.34	1.64	7.03	5.8
0.5-K-CLN	73.04	12.66	0.76	0.25	0.23	0.62	6.38	5.97	5.8
1.0-K-CLN	73.72	12.49	0.68	0.18	0.23	0.61	6.40	5.68	5.9
0.5-Ca-CLN	73.47	12.05	0.72	0.16	2.10	–	1.59	9.35	6.1
1.0-Ca-CLN	74.53	12.51	0.72	0.15	2.25	0.77	1.69	7.38	5.9
0.5-Mg-CLN	74.58	12.90	0.76	1.09	0.22	0.52	1.70	8.18	5.8
1.0-Mg-CLN	74.75	12.79	0.68	1.12	0.26	0.52	1.83	8.04	5.8

Compared to raw CLN, the relative peak intensity of (200) for the parent CLN and other cation-exchanged forms decreased relative to the peak intensity of (020), except for the 0.5-K-CLN and 1.0-K-CLN samples. The changes in the absolute and relative intensities of the characteristic peaks of the CLN samples can be attributed to the changes in the atomic positions and atomic densities in the structure and in the pore size and pore shape of the CLN (Galli *et al.*, 1983; Castaldi *et al.*, 2008; Kennedy & Tezel, 2018; Rodríguez-Iznaga *et al.*, 2022). The relative changes in the peak intensities from our XRD results can be attributed to changes in the exchangeable cation ratios, as shown in the XRF data (Table 1), as the intensity of the (020) peak is highly dependent on the Na/K ratio of the CLN samples (Kitsopoulos, 2001). Furthermore, the absence of a broad hump between 19° and 30°2θ for the CLN and cation-exchanged forms indicates that the method used in this study did not damage the CLN structure, unlike other modification methods such as acid treatment (Arcoya *et al.*, 1994; Christidis *et al.*, 2003; Garcia-Basabe *et al.*, 2010; Kennedy & Tezel, 2018).

The unit-cell parameters (*a*, *b*, *c* and β) and volumes of the CLN samples obtained from the *h*, *k* and *l* dimensions in the monoclinic crystal structure are listed in Table 2. A decrease in the unit-cell volume value of the parent sample compared to the raw sample was observed. This decrease due to calcination is similar that observed in other studies focused on CLN (Kudoh & Takéuchi, 1983; Bish, 1984; Tomazović *et al.*, 1996a, 1996b). In addition, the unit-cell volume values of all cation-doped forms were larger than the unit-cell volume of the parent sample.

SEM observations

SEM images taken at magnifications of at 5000× and 14 000× for the raw CLN, parent CLN, 0.5-Na-CLN, 0.5-K-CLN, 0.5-Ca-CLN,

https://doi.org/10.1180/clm.2024.5 Published online by Cambridge University Press

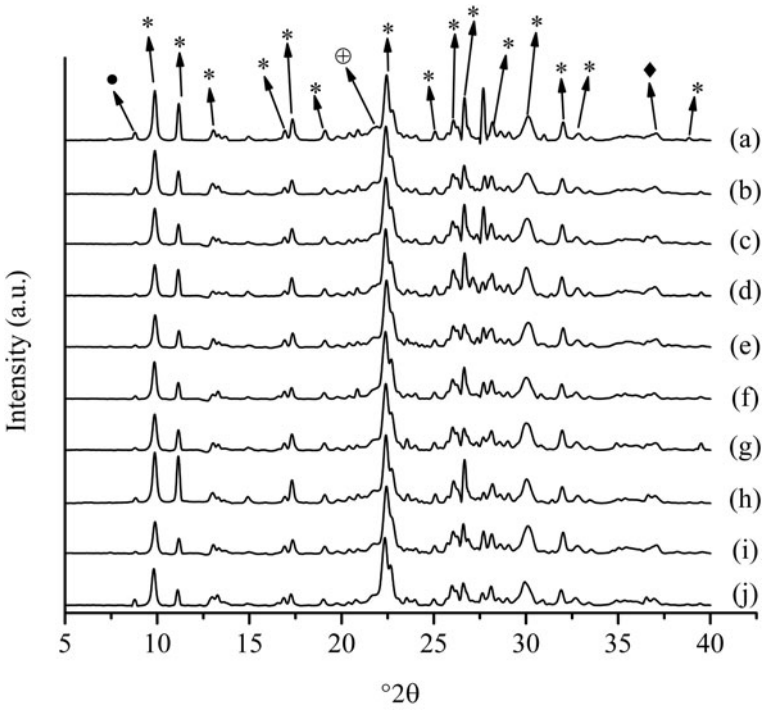

Figure 2. XRD traces of the zeolites. (a) Raw-CLN, (b) parent-CLN, (c) 0.5-Na-CLN, (d) 0.5-K-CLN, (e) 0.5-Ca-CLN, (f) 0.5-Mg-CLN, (g) 1.0-Na-CLN, (h) 1.0-K-CLN, (i) 1.0-Ca-CLN, (j) 1.0-Mg-CLN. * = CLN, • = illite, ⊕ = opal A, ◆ = feldspar.

0.5-Mg-CLN, 1.0-Na-CLN, 1.0-K-CLN, 1.0-Ca-CLN and 1.0-Mg-CLN samples are shown in Figs 3 & 4. The CLN crystals form euhedral and subhedral plates, as well as coffin-shaped forms, in all samples (Figs 3 & 4a–e), similar to what has been observed in previous studies (Brundu & Cerri, 2015; Favvas *et al.*, 2016; Fajdek-Bieda *et al.*, 2021). HEU-type crystals have platy, tabular or coffin habits (Elaiopoulos *et al.*, 2010). In addition, some submicron and irregularly shaped CLN grains are also seen in all SEM images. The size of the crystals is consistent with that of the mineral obtained from the same region (Ünaldi *et al.*, 2013).

N_2 adsorption

The N_2 adsorption isotherms measured at 77 K are shown in Figs 5 & 6. The specific surface areas, micropore areas and micropore volumes of all of the samples were determined using the Brunauer–Emmett–Teller (BET) and the *t*-plot methods, respectively (Table 3). All isotherms are of type II according to the International Union of Pure and Applied Chemistry (IUPAC; Lowell *et al.*, 2004). The knee portion of the isotherm indicates the stage when the coverage of the monolayer is complete and multilayer adsorption begins to take place (Helminen *et al.*, 2001; Lowell *et al.*, 2004). The parent CLN has a higher specific surface area (106.93 m^2 g^{-1}), micropore area (81.27 m^2 g^{-1}) and micropore volume (0.0317 cm^3 g^{-1}) than the raw CLN sample (Table 3). This can be explained by the removal of exchangeable cations (K^+, Na^+, Mg^{2+} and Ca^{2+}) from the structure due to the method used in the study, the preservation of the H^+ form without damaging the crystal structure and the easier diffusion of nitrogen. Similar increases in the BET values have been observed for an NH_4NO_3-exchanged CLN from Germany (Hieu *et al.*, 2022) and an NH_4Cl-exchanged CLN from Bigadiç, Türkiye (Kurama *et al.*, 2002). In addition, the BET surface areas of the cation-exchanged samples showed wide variation, in the range of 30.72–198.98 m^2 g^{-1}. The maximum specific surface area of the 1.0-Mg-CLN sample can be explained by the replacement of exchangeable cations such as Ca^{2+} and K^+ by Mg^{2+} (which is smaller in size), as is confirmed by the XRF data (Table 1).

Table 2. Unit-cell parameters and volumes for raw CLN and parent CLN and its cation-exchanged forms.

Sample	*a* (Å)	*b* (Å)	*c* (Å)	β (°)	*V* (Å^3)
Raw CLN	17.775	17.904	7.409	117.20	2097
Parent-CLN	17.759	17.830	7.398	116.97	2088
0.5-Na-CLN	17.789	17.904	7.414	117.13	2101
1.0-Na-CLN	17.754	17.904	7.412	116.91	2101
0.5-K-CLN	17.766	17.924	7.404	116.92	2102
1.0-K-CLN	17.745	17.904	7.402	116.86	2098
0.5-Ca-CLN	17.784	17.868	7.409	117.14	2095
1.0-Ca-CLN	17.770	17.868	7.406	117.10	2093
0.5-Mg-CLN	17.802	17.942	7.411	117.08	2108
1.0-Mg-CLN	17.799	17.998	7.419	117.05	2117

Ammonia adsorption

Direct or indirect ion exchange with NH_4NO_3 followed by employing the calcination method can be applied to zeolite-type materials because this process removes the exchangeable cations whilst leaving the structure unaffected, unlike the methods involving solutions of HCl or H_2SO_4, which cause structure decomposition. In this study, the direct and indirect ammonium nitrate treatment methods before calcination were carried out using multiple molarities (0.5 and 1.0 M). The 0.5-4h-CLN (3.95 mmol g^{-1}), 0.5-8h-CLN (4.02 mmol g^{-1}), 1.0-4h-CLN (3.99 mmol g^{-1}) and 1.0-8h-CLN (3.92 mmol g^{-1}) samples in which the H^+ forms were obtained directly without conversion to the Na^+ form, defined as Method 1, adsorbed less ammonia than the Na-0.5-4h-CLN (4.19 mmol g^{-1}), Na-0.5-8h-CLN (4.07 mmol g^{-1}), Na-1.0-4h-CLN (4.10 mmol g^{-1}) and Na-1.0-8h-CLN (4.46 mmol g^{-1})

https://doi.org/10.1180/clm.2024.5 Published online by Cambridge University Press

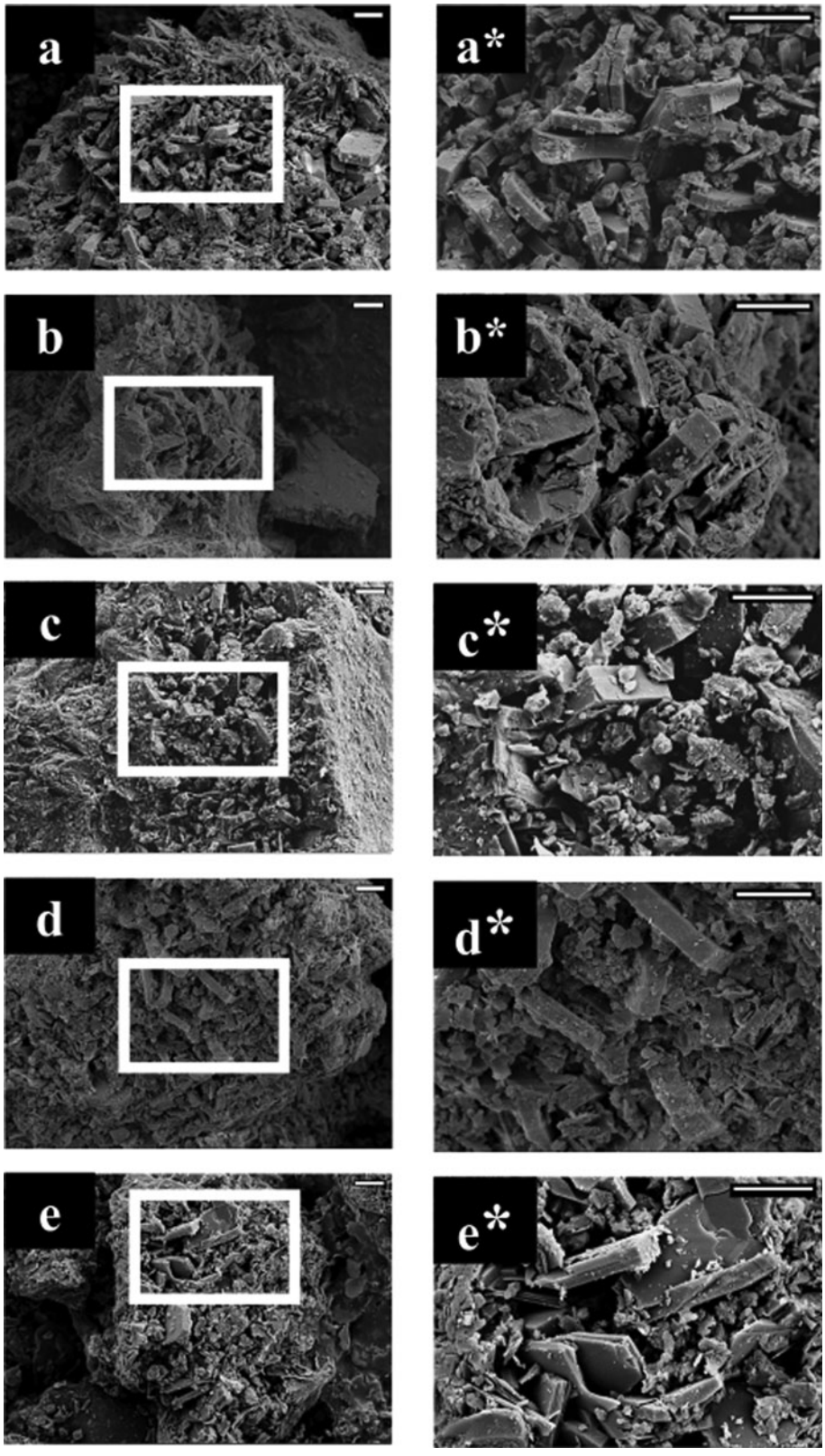

Figure 3. SEM images of (a) raw-CLN, (b) 0.5-Na-CLN, (c) 0.5-K-CLN, (d) 0.5-Ca-CLN and (e) 0.5-Mg-CLN at a magnification of 5000×. Letter labels with a * symbol corresponds to 14,000× magnification.

samples obtained using Method 2. In these H^+ forms obtained by the two methods, the removal of exchangeable Mg^{2+}, Ca^{2+} and Na^+ cations by direct or indirect ion exchange with NH_4NO_3, followed by calcination, caused a general decrease in the ammonia adsorption capacities compared to the raw sample. For this reason, Na-1.0-8h, which has the highest ammonia adsorption capacity amongst the H^+ forms, was selected as the parent sample. The next step was to determine the ammonia adsorption capacities by doping the parent sample with different cations. The ammonia adsorption isotherms of the raw CLN, the parent sample and that

https://doi.org/10.1180/clm.2024.5 Published online by Cambridge University Press

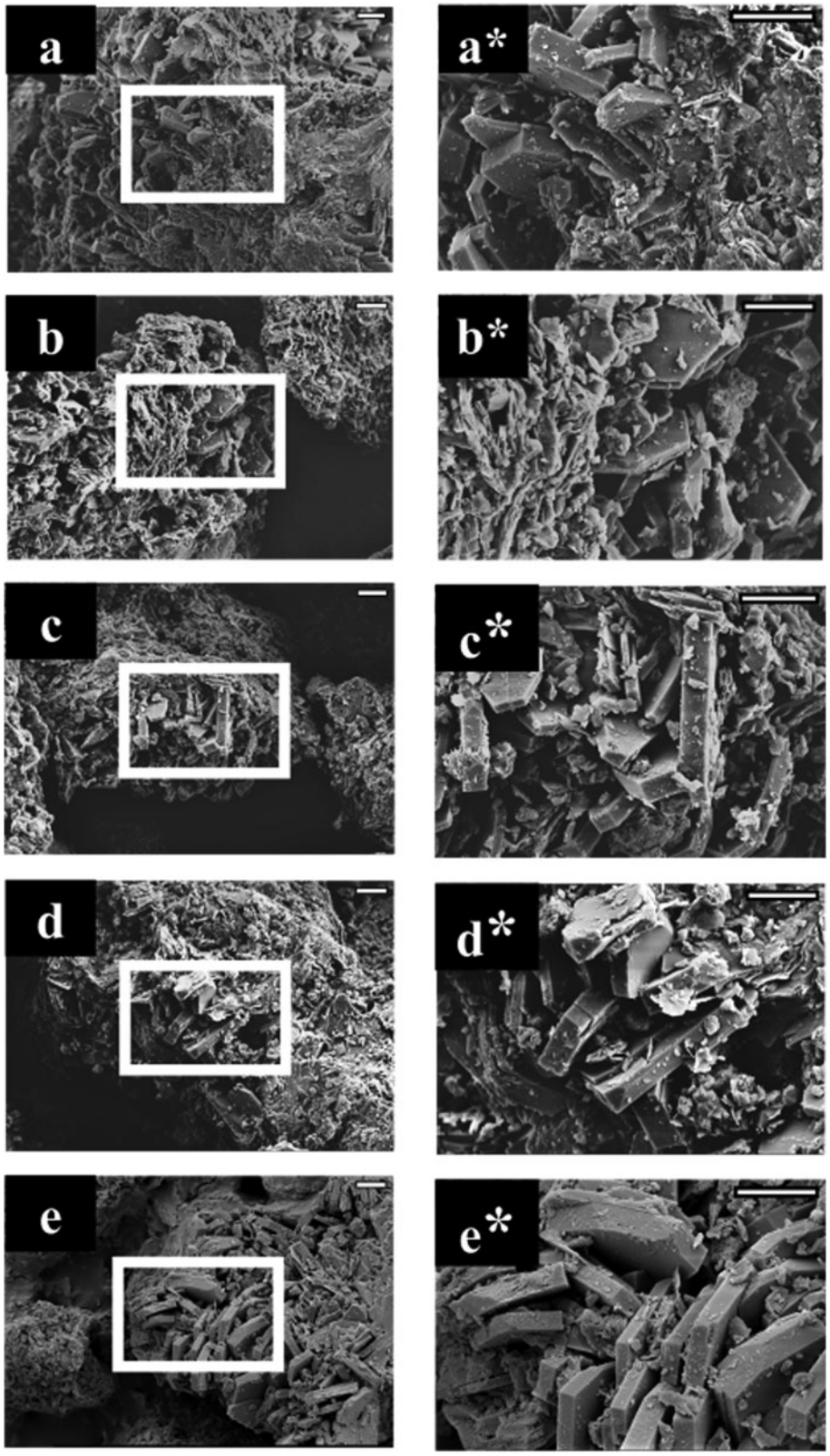

Figure 4. SEM images of (a) parent-CLN, (b) 1.0-Na-CLN, (c) 1.0-K-CLN, (d) 1.0-Ca-CLN and (e) 1.0-Mg-CLN at a magnification of 5000×. Letter labels with a * symbol corresponds to 14,000× magnification.

of cation-exchanged forms at 298 K up to a pressure of 100 kPa are shown in Figs 7 & 8.

The ammonia uptake of the CLN samples ranged from 3.61 to 4.93 mmol g^{-1} and increased in the following order: 1.0-K-CLN < 0.5-K-CLN < 1.0-Mg-CLN < 1.0-Na-CLN < 0.5-Mg-CLN < raw CLN < parent CLN < 1.0-Ca-CLN < 0.5-Ca-CLN < 0.5-Na-CLN (Table 4). When the molarity of the salt solutions used was two times higher (from 0.5 to 1.0 M), the ammonia adsorption capacity decreased. The raw CLN sample showed lower ammonia uptake (4.41 mmol g^{-1}) compared to CLN from

https://doi.org/10.1180/clm.2024.5 Published online by Cambridge University Press

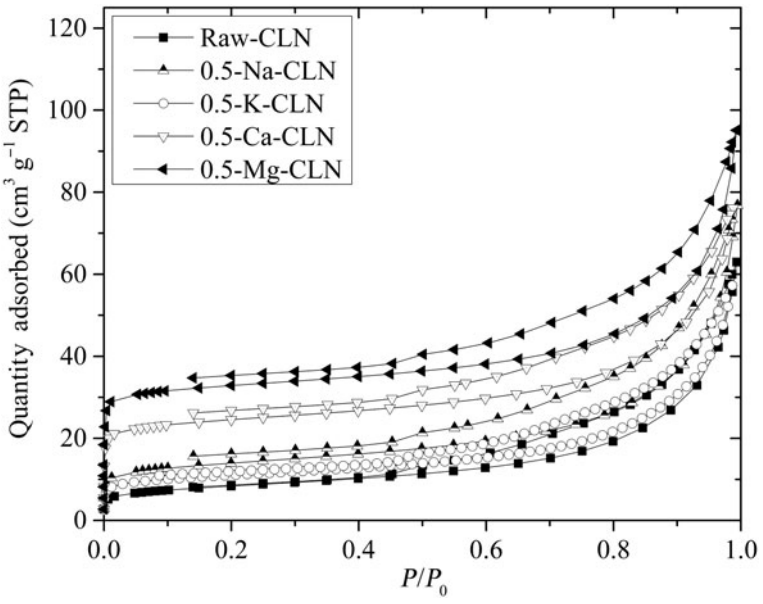

Figure 5. N_2 adsorption isotherms of raw CLN, 0.5-Na-CLN, 0.5-K-CLN, 0.5-Ca-CLN and 0.5-Mg-CLN samples at 77 K. STP = standard temperature and pressure.

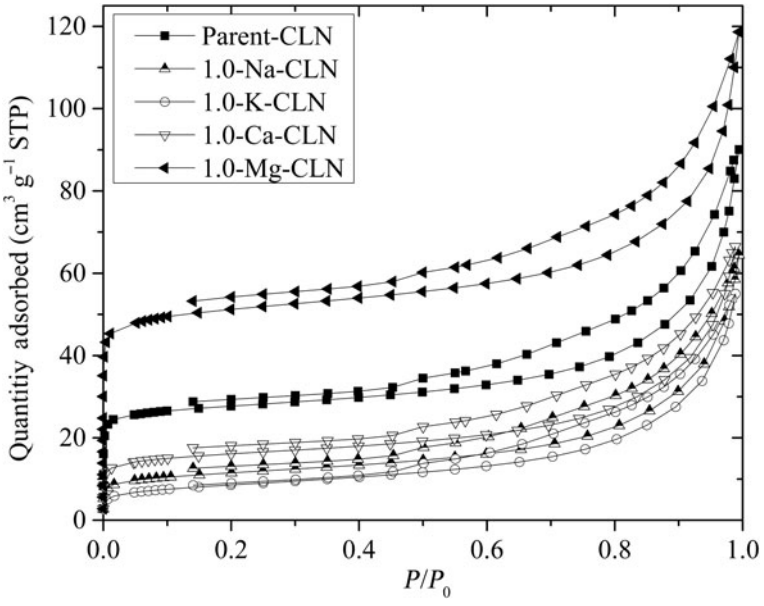

Figure 6. N_2 adsorption isotherms of parent CLN, 1.0-Na-CLN, 1.0-K-CLN, 1.0-Ca-CLN and 1.0-Mg-CLN samples at 77 K. STP = standard temperature and pressure.

Table 3. N_2 adsorption data of the raw CLN and parent CLN and its cation-exchanged forms.

Sample	BET surface area (m^2 g^{-1})	Micropore surface area (m^2 g^{-1})	Micropore volume ($\times 10^{-2}$ cm^3 g^{-1})
Raw CLN	30.08	8.53	0.35
Parent-CLN	106.93	81.27	3.17
0.5-Na-CLN	49.76	23.70	1.02
0.5-K-CLN	39.98	17.77	0.74
0.5-Ca-CLN	93.15	67.75	2.69
0.5-Mg-CLN	127.03	100.26	3.92
1.0-Na CLN	42.01	20.09	0.82
1.0-K-CLN	30.72	8.46	0.35
1.0-Ca-CLN	60.04	37.05	1.49
1.0-Mg-CLN	198.98	163.36	6.36

Mud Hills, USA (5.90 mmol g^{-1}; Helminen *et al.*, 2001) but a higher uptake than the Slovakian CLN (0.71 mmol g^{-1}; Ciahotný *et al.*, 2006) due to its different mineralogical and chemical composition. Although the specific surface area (106.93 m^2 g^{-1}) and micropore surface area (81.27 m^2 g^{-1}) values of the parent CLN were higher than those of the cation-exchanged forms (30.72–93.15 m^2 g^{-1} and 8.46–67.75 m^2 g^{-1}) with 0.5 and 1.0 M $NaNO_3$, KNO_3 and $Ca(NO_3)_2$ solutions, respectively (Table 4), it showed an average ammonia adsorption capacity. This can be attributed to the significant removal of exchangeable cations in the parent sample, in one of the H-forms obtained using Method 2. This also clearly demonstrates the influence of the extra-framework cations on ammonia adsorption and the interactions of the permanent dipole moment (1.47 Debye) of the ammonia molecule with the electric field generated by these

https://doi.org/10.1180/clm.2024.5 Published online by Cambridge University Press

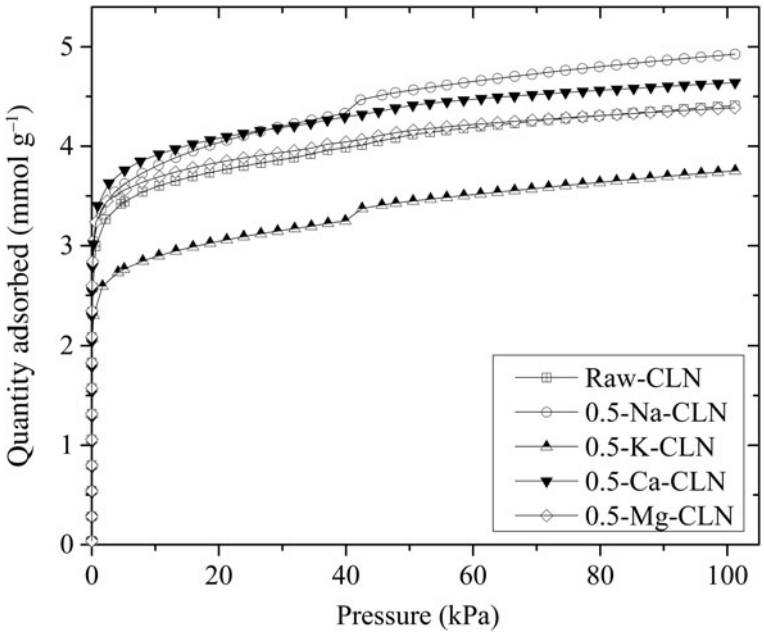

Figure 7. NH_3 adsorption isotherms of raw CLN, 0.5-Na-CLN, 0.5-K-CLN, 0.5-Ca-CLN and 0.5-Mg-CLN samples at 298 K.

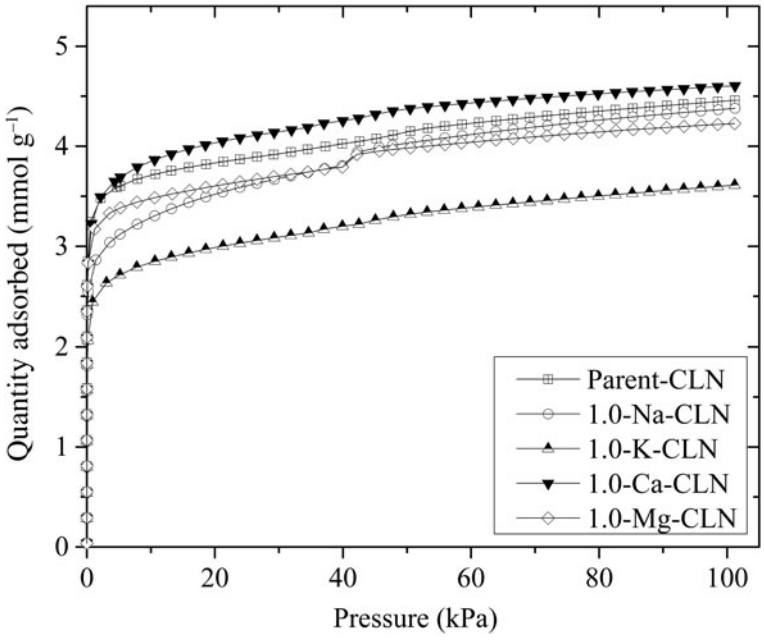

Figure 8. NH_3 adsorption isotherms of parent CLN, 1.0-Na-CLN, 1.0-K-CLN, 1.0-Ca-CLN and 1.0-Mg-CLN samples at 298 K.

cations. Amongst the cation-modified forms of the parent sample, 0.5-Na-CLN (4.93 mmol g^{-1}) showed the highest uptake. This result for the 0.5-Na-CLN sample showed that it is beneficial to dope the parent sample with Na^+ cation in a second step. As shown in Fig. 9, in CLN, Na^+, Ca^{2+} and K^+ cations prefer to occupy sites M(1) (in channel A), M(2) (in channel B) and M (3) (in channel C), respectively, whereas the Mg^{2+} cation is located at site M(4) (in channel A; Koyama & Takeuchi, 1977). The exchange of Na^+ cations with Mg^{2+}, Ca^{2+} and K^+ cations and the presence of these smaller Na^+ cations in the M(1) site of channel A resulted in there being a larger area within the channels. On the other hand, the 1.0-K-CLN sample had both the lowest specific surface area (30.72 m^2 g^{-1}) and the lowest ammonia adsorption capacity (3.61 mmol g^{-1}) due to the size and position of the K^+ (largest) cation and partial pore blocking that occurred. The percentage change in the ammonia adsorption capacity of the parent and the cation-exchanged forms compared to the natural sample ranged between 0.45 and 18.14.

The ammonia adsorption capacity of the 0.5-Na-CLN sample (4.93 mmol g^{-1}) is lower than that of MOF-177 (12.2 mmol g^{-1}; Saha & Deng, 2010b), 13X (9.33 mmol g^{-1}; Helminen *et al.*, 2001), 4A (8.71 mmol g^{-1}; Helminen *et al.*, 2001) and mesoporous carbon (6.39 mmol g^{-1}; Saha & Deng, 2010a) but higher than those of activated alumina (2.53 mmol g^{-1}; Saha & Deng,

https://doi.org/10.1180/clm.2024.5 Published online by Cambridge University Press

Table 4. Comparison of the removal of ammonia at 298 K in this study with materials from previous studies.

Sample	Adsorption capacity (mmol g^{-1})	Pressure (kPa)	Reference
Raw CLN	4.41 ± 0.22		Present work
Parent-CLN	4.46 ± 0.08		Present work
0.5-Na-CLN	4.93 ± 0.12		Present work
1.0-Na CLN	4.38 ± 0.00		Present work
0.5-K-CLN	3.75 ± 0.19		Present work
1.0-K-CLN	3.61 ± 0.00	101	Present work
0.5-Ca-CLN	4.64 ± 0.09		Present work
1.0-Ca-CLN	4.61 ± 0.04		Present work
0.5-Mg-CLN	4.39 ± 0.09		Present work
1.0-Mg-CLN	4.23 ± 0.13		Present work
CLN (USA)	5.90	101	Helminen *et al.* (2001)
CLN (Slovakia)	0.71 (12.2 mg g^{-1})	Fixed bed	Ciahotný *et al.* (2006)
MOF-177	12.20	106	Saha & Deng (2010b)
13X	9.33	101	Helminen *et al.* (2001)
4A	8.71	101	Helminen *et al.* (2001)
Mesoporous carbon	6.39	106	Saha & Deng (2010a)
Dealuminated pentasil	2.34	101	Helminen *et al.* (2001)
Cu-MOF-74	3.40	Breakthrough	Katz *et al.* (2016)
Activated alumina	2.53	108	Saha & Deng (2010c)
Activated carbon	4.19	101	Helminen *et al.* (2001)
Faujasite (dealuminated)	1.77	101	Helminen *et al.* (2001)

2010c), dealuminated pentasil (2.34 mmol g^{-1}; Helminen *et al.*, 2001), activated carbon (4.19 mmol g^{-1}; Helminen *et al.*, 2001), dealuminated faujasite (1.77 mmol g^{-1}; Helminen *et al.*, 2001) and Cu-MOF-74 (3.4 mmol g^{-1}; Katz *et al.*, 2016; Table 4). Comparing the ammonia adsorption data obtained at the same temperature (Table 4), it is clear that the structural and textural properties of these synthetic materials are completely different from natural zeolite of the CLN type. Although in general the synthetic zeolites, due to their uniform structure, have higher gas adsorption capacities than natural zeolites, they are more expensive. The abundance of CLN-type natural zeolite, its low cost and its high capacity to adsorb harmful gases such as ammonia lead to its widespread use in industrial applications. As a result, the 0.5-Na-CLN sample with the highest ammonia adsorption capacity is recommended as an effective adsorbent in environments where ammonia gas needs to be removed, such as poultry houses.

Conclusions

In this study, the structural properties and ammonia adsorption capacities of the parent CLN and its forms doped with Na^+, K^+, Ca^{2+} and Mg^{2+} cations were compared. The XRD data of the CLN samples showed that the NH_4NO_3 modification and the

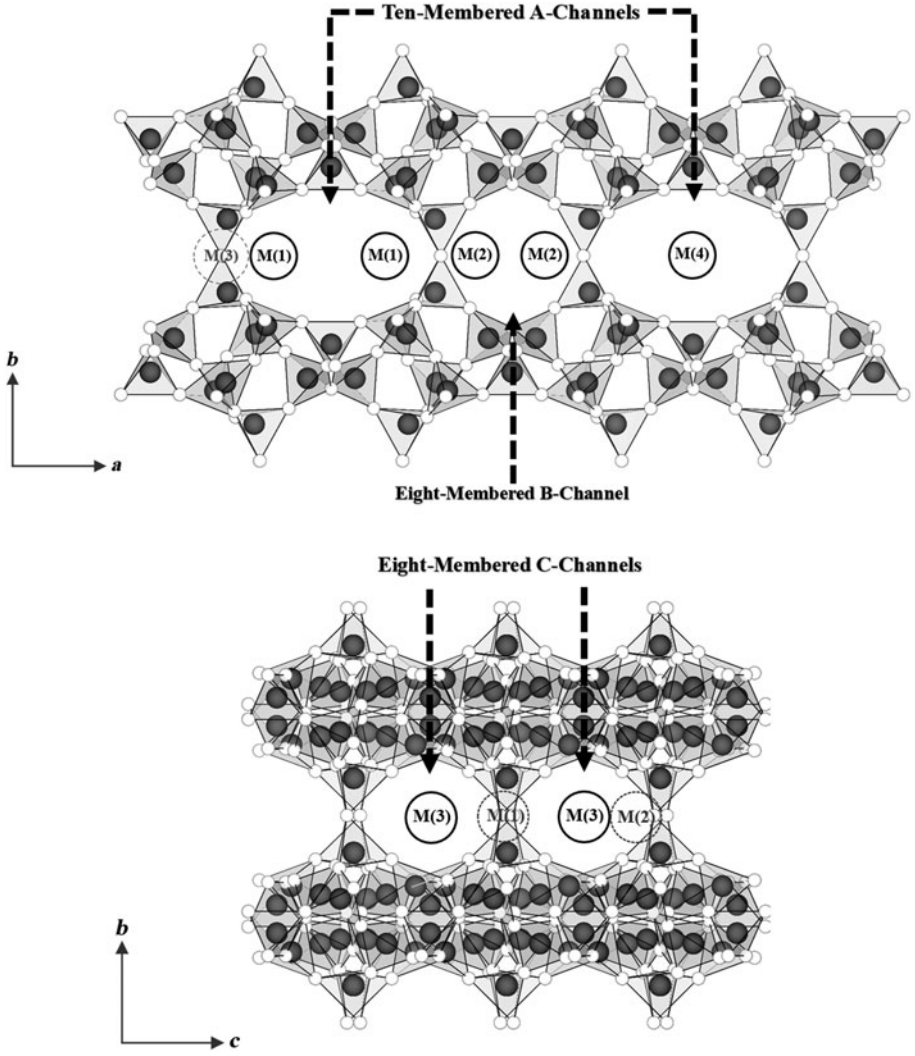

Figure 9. Views of the CLN framework and cation sites along the *c*-axis and *a*-axis.

https://doi.org/10.1180/clm.2024.5 Published online by Cambridge University Press

calcination process to obtain the H^+ forms prior to the cation exchange did not cause any significant damage to the crystal structure. It was also found that the morphology of the modified samples was not affected by calcining. A more than threefold increase in BET surface area (106.93 m^2 g^{-1}) was observed for the parent sample compared to the raw CLN (30.08 m^2 g^{-1}). CLN samples in which the H^+ forms were obtained by first converting to the Na^+ form (as a result of ammonium nitrate and calcination), as defined by Method 2, adsorbed more ammonia than directly obtained H^+ forms, as defined by Method 1. A wide variation in ammonia adsorption was observed in the cation-exchanged CLNs, being more dependent on the size, amount and location of the exchanged cation than on the BET surface areas. Consequently, 0.5-Na-CLN, which has the highest ammonia adsorption capacity amongst the samples used in this study, can be suggested as a potential material for ammonia removal applications.

Acknowledgements. The authors thank Ceramic Research Center (SAM, Eskisehir/Turkey) for the XRF analysis of all samples.

Financial support. Financial support from Eskisehir Technical University Scientific Research Committee under grant number 22ADP355 is gratefully acknowledged.

Conflicts of interest. The authors declare none.

References

Allen S.J., Ivanova E. & Koumanova B. (2009) Adsorption of sulfur dioxide on chemically modified natural clinoptilolite. Acid modification. *Chemical Engineering Journal*, **152**, 389–395.

Ambrozova P., Kynicky J., Urubek T. & Nguyen V.D. (2017) Synthesis and modification of clinoptilolite. *Molecules*, **22**, 1107.

Amon M., Dobeic M., Sneath R.W., Phillips V.R., Misselbrook T.H. & Pain B.F. (1997) A farm-scale study on the use of clinoptilolite zeolite and De-Odorase® for reducing odour and ammonia emissions from broiler houses. *Bioresource Technology*, **61**, 229–237.

Arcoya A., González J.A., Travieso N. & Seoane X.L. (1994) Physicochemical and catalytic properties of a modified natural clinoptilolite. *Clay Minerals*, **29**, 123–131.

Ballal S.G., Ali B.A., Albar A.A., Ahmed H.O. & Al-Hasan A.Y. (1998) Bronchial asthma in two chemical fertilizer producing factories in eastern Saudi Arabia. *International Journal of Tuberculosis and Lung Disease*, **2**, 330–335.

Bish D.L. (1984) Effects of exchangeable cation composition on the thermal expansion/contraction of clinoptilolite. *Clays and Clay Minerals*, **32**, 444–452.

Brundu A., & Cerri G. (2015) Thermal transformation of Cs-clinoptilolite to $CsAlSi_5O_{12}$. *Microporous and Mesoporous Materials*, **208**, 44–49.

Castaldi P., Santona L., Enzo S. & Melis P. (2008) Sorption processes and XRD analysis of a natural zeolite exchanged with Pb^{2+}, Cd^{2+} and Zn^{2+} cations. *Journal of Hazardous Materials*, **156**, 428–434.

Christidis G.E., Moraetis D., Keheyan E., Akhalbedashvili L., Kekelidze N., Gevorkyan R. *et al.* (2003) Chemical and thermal modification of natural HEU-type zeolitic materials from Armenia, Georgia and Greece. *Applied Clay Science*, **24**, 79–91.

Ciahotný K., Melenová L., Jirglová H., Boldiš M. & Kočiřík M. (2002) Sorption of ammonia from gas streams on clinoptilolite impregnated with inorganic acids. *Studies in Surface Science and Catalysis*, **142B**, 1713–1720.

Ciahotný K., Melenová L., Jirglová H., Pachtová O., Kočiřík M. & Eić M. (2006) Removal of ammonia from waste air streams with clinoptilolite tuff in its natural and treated forms. *Adsorption*, **12**, 219–226.

Drummond J.G., Curtis S.E., Simon J. & Norton H.W. (1980) Effects of aerial ammonia on growth and health of young pigs. *Journal of Animal Science*, **50**, 1085–1091.

Dziedzicka A., Sulikowski B. & Ruggiero-Mikołajczyk M. (2016) Catalytic and physicochemical properties of modified natural clinoptilolite, *Catalysis Today*, **259**, 50–58.

El-Arish N.A.S., Zaki R.S.R.M., Miskan S.N., Setiabudi H.D. & Jaafar N.F. (2022) Adsorption of Pb(II) from aqueous solution using alkaline-treated natural zeolite: process optimization analysis. *Total Environment Research Themes*, **3–4**, 100015.

Elaiopoulos K., Perraki T. & Grigoropoulou E. (2010) Monitoring the effect of hydrothermal treatments on the structure of a natural zeolite through a combined XRD, FTIR, XRF, SEM and N_2-porosimetry analysis. *Microporous and Mesoporous Materials*, **134**, 29–43.

Elboughdiri N. (2020) The use of natural zeolite to remove heavy metals Cu (II), Pb(II) and Cd(II), from industrial wastewater. *Cogent Engineering*, **7**, 1782623.

Elysabeth T., Zulnovri, Ramayanti G., Setiadi S. & Slamet S. (2019) Modification of Lampung and Bayah natural zeolite to enhance the efficiency of removal of ammonia from wastewater. *Asian Journal of Chemistry*, **31**, 873–878.

Erdoğan Alver B. & Sakızcı M. (2019) Hydrogen (H_2) adsorption on natural and cation-exchanged clinoptilolite, mordenite and chabazite. *International Journal of Hydrogen Energy*, **44**, 6748–6755.

Esenli F. & Sirkecioğlu A. (2005) The relationship between zeolite (heulandite–clinoptilolite) content and the ammonium-exchange capacity of pyroclastic rocks in Gördes, Turkey. *Clay Minerals*, **40**, 557–564.

Esenli F., Ekinci Şans B., Erdoğan B. & Sirkecioğlu A. (2023) The surface characteristics of natural heulandites/clinoptilolites with different extra-framework cations. *Clay Minerals*, **58**, https://doi.org/10.1180/clm.2023.34.

Fajdek-Bieda A., Wróblewska A., Miądlicki P., Tołpa J. & Michalkiewicz B. (2021) Clinoptilolite as a natural, active zeolite catalyst for the chemical transformations of geraniol. *Reaction Kinetics, Mechanisms and Catalysis*, **133**, 997–1011.

Favvas E.P., Tsanaktsidis C.G., Sapalidis A.A., Tzilantonis G.T., Papageorgiou S.K. & Mitropoulos A.C. (2016) Clinoptilolite, a natural zeolite material: structural characterization and performance evaluation on its dehydration properties of hydrocarbon-based fuels. *Microporous and Mesoporous Materials*, **225**, 385–391.

Fowler D., Brimblecombe P., Burrows J., Heal M.R., Grennfelt P., Stevenson D.S. *et al.* (2020) A chronology of global air quality. *Philosophical Transactions of the Royal Society A*, **378**, 20190314.

Galli E., Gottardi G., Mayer H., Preisinger A. & Passaglia E. (1983) The structure of potassium-exchanged heulandite at 293, 373 and 593 K. *Acta Crystallographica Section B*, **39**, 189–197.

Garcia-Basabe Y., Rodriguez-Iznaga I., de Menorval L.C., Llewellyn P., Maurin G., Lewis D.W. *et al.* (2010) Step-wise dealumination of natural clinoptilolite: Structural and physicochemical characterization. *Microporous and Mesoporous Materials*, **135**, 187–196.

Ghahri A., Golbabaei F., Vafajoo L., Mireskandari S.M., Yaseri M. & Shahtaheri S.J. (2017) Removal of greenhouse gas (N_2O) by catalytic decomposition on natural clinoptilolite zeolites impregnated with cobalt, *International Journal of Environmental Research*, **11**, 327–337.

Gottardi G. & Galli E. (1985) *Natural Zeolites*. Springer, Berlin, Germany, 411 pp.

Helminen J., Helenius J., Paatero E. & Turunen I. (2001) Adsorption equilibria of ammonia gas on inorganic and organic sorbents at 298.15 K, *Journal of Chemical Engineering Data*, **46**, 391–399.

Hieu D.T., Kosslick H., Riaz M., Schulz A., Springer A., Frank M. *et al.* (2022) Acidity and stability of Brønsted acid sites in green clinoptilolite catalysts and catalytic performance in the etherification of glycerol. *Catalysts*, **12**, 253.

Karousos D.S., Sapalidis A.A., Kouvelos E.P., Romanos G.E. & Kanellopoulos N.K. (2016) A study on natural clinoptilolite for CO_2/N_2 gas separation. *Separation Science and Technology*, **51**, 83–95.

Katz M.J., Howarth A.J., Moghadam P.Z., DeCoste J.B., Snurr R.Q., Hupp J.T. & Farha O.K. (2016) High volumetric uptake of ammonia using Cu-MOF-74/Cu-CPO-27. *Dalton Transactions*, **45**, 4150–4153.

Kennedy D.A. & Tezel, F.H. (2018) Cation exchange modification of clinoptilolite – screening analysis for potential equilibrium and kinetic adsorption separations involving methane, nitrogen, and carbon dioxide. *Microporous and Mesoporous Materials*, **262**, 235–250.

https://doi.org/10.1180/clm.2024.5 Published online by Cambridge University Press

Kitsopoulos K.P. (2001) The relationship between the thermal behavior of clinoptilolite and its chemical composition. *Clays and Clay Minerals*, **49**, 236–243.

Kobayashi H., Hayakawa A., Somarathne K.D.K.A. & Okafor E.C. (2019) Science and technology of ammonia combustion. *Proceedings of the Combustion Institute*, **37**, 109–133.

Koyama K. & Takeuchi Y. (1977) Clinoptilolite: the distribution of potassium atoms and its role in thermal stability. *Zeitschrift Für Kristallographie-Crystalline Materials*, **145**, 216–239.

Kudoh Y. & Takéuchi Y. (1983) Thermal stability of clinoptilolite: the crystal structure at 350 °C. *Mineralogical Journal*, **11**, 392–406.

Kurama H., Zimmer A. & Reschetilowski W. (2002) Chemical modification effect on the sorption capacities of natural clinoptilolite. *Chemical Engineering & Technology*, **25**, 301–305.

Li J., Chang H., Ma L., Hao J. & Yang R.T. (2011) Low-temperature selective catalytic reduction of NO_x with NH_3 over metal oxide and zeolite catalysts – a review. *Catalysis Today*, **175**, 147–156.

Liao J., Zhang Y., Fan L., Chang L. & Bao W. (2019) Insight into the acid sites over modified NaY zeolite and their adsorption mechanisms for thiophene and benzene. *Industrial & Engineering Chemistry Research*, **58**, 4572–4580.

Lindgren T. (2010) A case of indoor air pollution of ammonia emitted from concrete in a newly built office in Beijing. *Building and Environment*, **45**, 596–600.

Lowell S., Shields J.E., Thomas M.A. & Thommes M. (2004) *Characterization of Porous Solids and Powders: Surface Area, Pore Size and Density*. Kluwer Academic Publishers, Dordrecht, The Netherlands, 349 pp.

Macala J., Pandova I., & Panda A. (2009) Clinoptilolite as a mineral usable for cleaning of exhaust gases. *Gospodarka Surowcami Mineralnymi*, **25**, 23–32.

Mastinu A., Kumar A., Maccarinelli G., Bonini S.A., Premoli M., Aria F. *et al.* (2019) Zeolite clinoptilolite: therapeutic virtues of an ancient mineral, *Molecules*, **24**, 1517.

Moore D.M. & Reynolds Jr R.C. (1997) *X-Ray Diffraction and the Identification and Analysis of Clay Minerals*, 2nd edition. Oxford University Press, New York, NY, USA, 400 pp.

Mumpton F.A. (1960) Clinoptilolite redefined. *American Minerologist*, **45**, 351–369.

Renard J.J., Calidonna S.E. & Henley M.V. (2004) Fate of ammonia in the atmosphere – a review for applicability to hazardous releases. *Journal of Hazardous Materials*, **108**, 29–60.

Rodríguez-Iznaga I., Shelyapina M.G. & Petranovskii V. (2022) Ion exchange in natural clinoptilolite: aspects related to its structure and applications. *Minerals*, **12**, 1628.

Rožić M. Cerjan-Stefanović Š., Kurajica S., Maěefat M.R., Margeta K. & Farkaš A. (2005) Decationization and dealumination of clinoptilolite tuff and ammonium exchange on acid-modified tuff. *Journal of Colloid and Interface Science*, **284**, 48–56.

Saha D. & Deng S. (2010a) Adsorption equilibrium and kinetics of CO_2, CH_4, N_2O, and NH_3 on ordered mesoporous carbon. *Journal of Colloid and Interface Science*, **345**, 402–409.

Saha D. & Deng S. (2010b) Ammonia adsorption and its effects on framework stability of MOF-5 and MOF-177. *Journal of Colloid and Interface Science*, **348**, 615–620.

Saha D. & Deng S. (2010c) Characteristics of ammonia adsorption on activated alumina. *Journal of Chemical Engineering Data*, **55**, 5587–5593.

Senila M., Neag E., Cadar O., Hoaghia M.A., Roman M., Moldovan A. *et al.* (2022) Characteristics of volcanic tuff from Macicasu (Romania) and its capacity to remove ammonia from contaminated air. *Molecules*, **27**, 3503.

Shamshiri A., Alimohammadi V., Sedighi M., Jabbari E. & Mohammadi M. (2022) Enhanced removal of phosphate and nitrate from aqueous solution using novel modified natural clinoptilolite nanoparticles: process optimization and assessment. *International Journal of Environmental Analytical Chemistry*, **102**, 5994–6013.

Sun C., Hong S., Cai G., Zhang Y., Kan H., Zhao Z. *et al.* (2021) Indoor exposure levels of ammonia in residences, schools, and offices in China from 1980 to 2019: a systematic review. *Indoor Air*, **31**, 1691–1706.

Tomazović B., Ćeranić T. & Sijarić G. (1996a) The properties of the NH_4-clinoptilolite. Part 1. *Zeolites*, **16**, 301–308.

Tomazović B., Ćeranić T. & Sijarić G. (1996b) The properties of the NH_4-clinoptilolite. Part 2. *Zeolites*, **16**, 309–312.

Ünaldi T., Mizrak I. & Kadir S. (2013) Physicochemical characterisation of natural K-clinoptilolite and heavy-metal forms from Gördes (Manisa, western Turkey). *Journal of Molecular Structure*, **1054–1055**, 349–358.

Wang J., Zhao H., Haller G. & Li Y. (2017) Recent advances in the selective catalytic reduction of NO_x with NH_3 on Cu-chabazite catalysts. *Applied Catalysis B*, **202**, 346–354.

Ward R.L. & McKague H.L. (1994) Clinoptilolite and heulandite structural differences as revealed by multinuclear nuclear magnetic resonance spectroscopy. *Journal of Physical Chemistry*, **98**, 1232–1237.

Won Kang D., Eungyung Ju S., Won Kim D., Kang M., Kim H. & Seop Hong C. (2020) Emerging porous materials and their composites for NH_3 gas removal. *Advanced Science*, **7**, 2002142.

Zendelska A., Golomeova M., Jakupi Š., Lisičkov K., Kuvendžiev S. & Marinkovski M. (2018) Characterization and application of clinoptilolite for removal of heavy metal ions from water resources. *Geologica Macedonica*, **32**, 21–32.

https://doi.org/10.1180/clm.2024.5 Published online by Cambridge University Press